Co-published by
Institute of Fluid-Flow Machinery
Polish Academy of Sciences
Committee on Thermodynamics and Combustion
Polish Academy of Sciences

http://www.imp.gda.pl/archives-of-thermodynamics/

ARCHIVES OF THERMODYNAMICS

Non-Similar Analysis of MHD Ferro-Nanofluid Flow over an Exponential Stretching/Shrinking Sheet with Particle Effects

Md Sayeed Iftekhar Yousuf[a], Jahangir Alam[a], M.G. Murtaza[b*], Md Touhidul Islam[c], Md Jashim Uddin[d], Tasnim Ul Islam[a], Md Fazley Elahi[a]

[a]Department of Computer Science and Mathematics, Bangladesh Agricultural University, Mymensingh-2202, Bangladesh
[b]Department of Mathematics, Comilla University, Cumilla-3506, Bangladesh
[c]Department of Irrigation and Water Management, Bangladesh Agricultural University, Mymensingh-2202, Bangladesh
[d]Department of Applied Mathematics, Noakhali Science and Technology University, Noakhali-3814, Bangladesh
*Corresponding author email: murtaza@cou.ac.bd

Received: 22.12.2025; revised: 09.03.2026; accepted: 15.03.2026

Abstract

Biomagnetic nanofluids have attracted considerable attention because of their potential applications in biomedical engineering, particularly in drug delivery, cancer therapy, and thermal management systems. In the present study, a nonsimilar analysis of biomagnetic blood-based nanofluid containing multiwalled carbon nanotubes over an exponential stretching/shrinking sheet is investigated. The model incorporates several important physical effects, including a transverse magnetic field, viscous dissipation, suction/injection, particle volume fraction, particle radius, and particle spacing during nanoparticle–blood interaction. The governing partial differential equations are transformed using nonsimilarity transformations and solved numerically through the local nonsimilarity technique with the bvp4c solver in MATLAB. The effects of the physical parameters on velocity, temperature distribution, skin friction coefficient and local Nusselt number are analysed in detail. The results indicate that increasing the magnetic field parameter, particle radius and nanoparticle volume fraction significantly reduces the velocity profile while enhancing the temperature distribution. Moreover, an increase in particle spacing improves both velocity and temperature profiles. Quantitatively, the heat transfer rate decreases by approximately 23.46% and 8.83% in the stretching and shrinking cases, respectively, when the nanoparticle volume fraction increases from 0 to 0.1. Moreover, the skin friction coefficient increases by approximately 24.15% and 23.9% with the increasing magnetic field strength, while increasing the particle radius from 1 to 2 reduces the skin friction coefficient by approximately 16.52% and 33.18% in the stretching and shrinking cases, respectively. These findings provide useful insights for the design and optimisation of biomagnetic nanofluid systems in biomedical and thermal engineering applications.

Keywords: Biomagnetic fluid dynamics; Magnetohydrodynamics; Nanoparticles; Nonsimilarity; Particle radius

Vol. 47(2026), No. 2, 131–140; doi: 10.24425/ather.2026.158679

Cite this manuscript as: Yousuf, S.I.M., Alam, J., Murtaza, M.G., Islam, T.M., Uddin, J.M., Islam, T.U., & Elahi, F.M. (2026). Non-Similar Analysis of MHD Ferro-Nanofluid Flow over an Exponential Stretching/Shrinking Sheet with Particle Effects. *Archives of Thermodynamics*, 47(2), 131−140.

1. Introduction

The suspension of nanoparticles (usually ranging in size from 1 nm to 100 nm) in conventional fluids such as water, oils, blood or ethylene glycol is known as nanofluid, and it is a crucial field of research in fluid dynamics. These nanoparticles may significantly improve the fluid's thermal conductivity and heat transfer characteristics, making nanofluids ideal for a range of technical uses. In this context, a promising nexus between nanotechnology and biomedical research is blood-based nanofluid flow. Researchers want to improve drug delivery methods, provide novel diagnostic tools, and increase the usefulness of blood for therapeutic purposes by utilising the special qualities of nanoparticles. The integration of blood-based nanofluids in the biomedi-

Nomenclature

B_0 – magnetic field strength, T
C_p – heat capacity, J/(kg K)
Ec – Eckert number
h – particle interspacing, m
M – magnetic field parameter
Nu – Nusselt number
Pr – Prandtl number
R_p – particle radius, m
Re – Reynolds number
S – suction/injection parameter
T – temperature, K
u, v – velocity components along axial and normal directions, m/s

Greek symbols

η – pseudosimilarity variable
θ – dimensionless temperature
κ – thermal conductivity, W/(m K)
λ – stretching/shrinking parameter
μ – dynamic viscosity, kg/(m s)
ξ – nonsimilarity variable
ρ – blood density, kg/m^3
σ – electrical conductivity, S/m
ϕ – particle volume fraction

Subscripts and Superscripts

nf – nanofluid
w – wall
∞ – free-stream

Abbreviations and Acronyms

CNT – carbon nanotube
HAM – homotopy analysis method
MHD – magnetohydrodynamic
MWCNT – multiwalled carbon nanotubes
SWCNT – single-wall carbon nanotube

cal and engineering domains has intriguing prospects for improving performance and efficiency and tailoring therapeutics as research progresses.

Single-wall carbon nanotubes (SWCNTs) and multiwall carbon nanotubes (MWCNTs) are important components in the mathematical framework of blood-based hybrid nanofluid flow presented by Saeed et al. [1], which takes into account the electromagnetic field and coupling stress. The hybrid nanofluid model increased the heat transfer rate by 11.95%, according to previous studies. TiO_2+Ag/blood flow was numerically analysed by Alanazi et al. [2]. They discovered through computationnal use of the Runge–Kutta technique that the particle volume fraction significantly contributes to improved heat transmission. A blood-based Casson nanofluid flow that permits SWCNT and MWCNT particles over an extended sheet was covered by Mohamed et al. [3]. According to previous studies, compared with SWCNTs, MWCNTs significantly affect blood flow. The hybrid nanofluid stagnation fluid flow exposed to an expanding surface was investigated by Samat et al. [4] using carbon nanotubes. According to the study, magnetic fields are crucial for fluid transport behaviour, and whenever the magnetic field parameter is smaller than 1, several solutions to the problem may be found. Kerosene-based carbon nanotubes (CNTs) exhibit greater skin friction than do engine oil- and water-based CNTs, according to the mathematical model of homogeneous nanofluid flow of Khan et al. [5]. A MATLAB-based bvp4c-technique stagnation point flow of a CNT nanofluid along a curved surface was quantitatively examined by Khan et al. [6]. According to the study, when comparing SWCNTs to MWCNTs, the rate of heat transmission increased noticeably. Using water as the base fluid, Das et al. [7] investigated the effects of radiation and an external magnetic field on the unsteady flow of a three-dimensional hybrid nanofluid exposed to upward and downward rotating disks in the cases of SWCNT+Fe_3O_4 and MWCNT+Fe_3O_4. The numerical analysis reveals that, in comparison with that of SWCNT+Fe_3O_4, the rate of heat transmission for MWCNT+Fe_3O_4 is less than 0.35%.

A Levenberg–Marquardt multilayer artificial neural network was introduced by Priyadharshini and Archana [8] to investigate SWCNT-MWCNT/H_2O flows. The authors discovered that larger values of the volume fraction result in an increase in the thermal profile of the fluid behaviour system as a whole. Rehamn et al. [9] investigated the effects of slip circumstances and magnetic fields on blood/MWCNT behaviour while taking various fluid characteristics into account. Using the homotopy approach (homotopy analysis method – HAM), they reported that the Nusselt number increases in tandem with the volume friction, Eckert number and dynamic viscosity of the nanoparticles. Ramanuja et al. [10] investigated the effects of heat sources and thermal radiation on magnetohydrodynamic (MHD) blood-SWCNT flow and discovered that resistive impedance in the flow direction validates better findings in SWCNTs than in pure blood. A mathematical framework of TiO_2+Fe_3O_4+SiO_2/blood-based hybrid nanofluid flow subject to an extended curved surface was proposed by Nagaraja et al. [11]. The investigation revealed that the Prandtl number increases the system's total heat transfer rate. A thorough examination of SWCNTs/blood and MWCNTs/blood subjected to unstable Marangoni convection flow on a stretched surface was performed by Rehman et al. [12]. Increasing the stretching parameter values reduces fluid skin friction with the use of a computational process. A mathematical model of blood based CNT flows under Joule dissipation and viscous heating was developed by Nasir et al. [13]. They discovered that higher solid volume fractions for both types of CNTs increase the heat transfer rate to the blood vessel wall. El Glılı and Drıouıch [14] investigated the principles of electrically conducting water-based carbon nanotubes on an expanding sheet and discovered that MWCNTs had greater normal and tangential velocities than those of SWCNTs; the temperature distribution showed the opposite trend. In their discussion of MHD Casson ternary hybrid nanofluid slip flow over a surface expanded with convective heat, Mahanta and Sharma [15] reported that when the suction increases, the thickness of the boundary layer decreases.

Ahmad et al. [16] examined transient electroviscous flow between squeezing plates via a ternary hybrid nanofluid composed of silicon carbide, aluminium oxide, and multiwall carbon nanotubes dispersed in water. Their study demonstrated that the incorporation of multiple nanoparticles significantly enhances thermal transport compared with that of conventional nanofluids, particularly in the presence of thermal radiation and heat generation effects. Yasir et al. [17] investigated the radiative stagnation-point flow of cross fluid with gyrotactic microorganisms and highlighted the important role of the activation energy and heat source/sink mechanisms in modifying the thermal and concentration fields. Ahsan et al. [18] analysed stratified bioconvective Williamson nanofluid flow over a curved stretching surface under the influence of Joule heating, a magnetic field and nonlinear thermal radiation, and reported that the magnetic and Williamson parameters tend to suppress the velocity field, whereas the thermal parameters significantly alter the temperature distribution. Furthermore, Yasir et al. [19] conducted a comparative analysis of radiative magnetised flows of micropolar, Casson, and Maxwell fluids with melting heat transfer and demonstrated that thermal radiation markedly intensifies the temperature field, particularly in the Casson fluid. Kallem et al. [20] investigated magnetohydrodynamic hyperbolic tangent fluid flow over a nonlinear stretching sheet in a porous medium, highlighting the significant influence of magnetic field strength, chemical reactions and heat sources on flow and heat transfer characteristics. Biswas et al. [21] analysed thermomagnetic convection and entropy generation in a wavy porous cavity filled with a Cu-Al_2O_3/water hybrid nanofluid and reported that magnetic field intensity and wall undulations strongly affect hydrothermal transport behaviour. M and De [22] examined electroosmotic Maxwell nanofluid flow in a Darcy-Forchheimer porous medium considering the Soret and Dufour effects, and demonstrated that electromagnetic forces and cross-diffusion mechanisms play roles in controlling velocity, temperature and concentration fields.

Motivated by the above studies, the main objective of the present work is to investigate the nonsimilar flow and heat transfer characteristics of a biomagnetic blood-based nanofluid containing multiwalled carbon nanotubes (MWCNTs) over an exponentially stretching/shrinking sheet. The analysis considers the combined influence of the magnetic field parameters, nanoparticle volume fraction, particle radius, and particle spacing during nanoparticle–blood interactions. The novelty of this study lies in incorporating the effects of the particle radius and interparticle spacing within a nonsimilar biomagnetic nanofluid framework over an exponential stretching/shrinking surface. The governing nonlinear partial differential equations are solved via a local nonsimilarity technique with the MATLAB bvp4c solver. The effects of the governing parameters on the velocity, temperature, skin friction coefficient and local Nusselt number are examined in detail, providing useful insight into biomagnetic nanofluid transport relevant to biomedical and microscale thermal applications.

2. Mathematical formulation

A two-dimensional steady electrically conducting biomagnetic fluid with nanoparticles is considered along the exponentially stretching/shrinking sheet, as depicted in Fig. 1. For the current study, the following assumptions are taken into consideration:

- laminar flow,
- incompressible flow,
- MHD flow,
- blood is considered the base fluid,
- multiwalled carbon nanotubes (MWCNTs) are considered to have a spherical shape,
- slip conditions,
- nonsimilar flow,
- particle radius and interspacing is assumed, while interacting with blood.

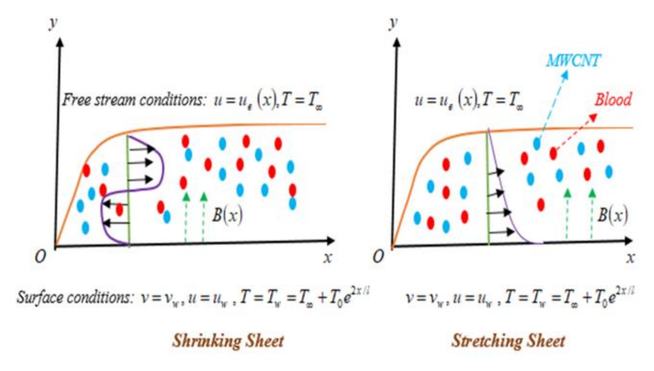

Fig. 1. Physical view of blood/MWCNT flow.

These assumptions define the physical framework of the present model and determine the range of applicability of the obtained results. The laminar and incompressible flow assumptions are appropriate for small-scale biomedical flow conditions where inertial and density variation effects are negligible. Therefore, the results obtained in this study apply to biomagnetic nanofluid transport systems, particularly in biomedical and microscale heat transfer applications where similar physical conditions exist.

Additionally, the sheet is considered to be stretched exponentially with velocity $u_w(x) = ce^{x/l}$ along the axial direction x, whereas the radial direction is denoted by y, where the stretching and shrinking cases are indicated by $c > 0$ and $c < 0$, respectively. The free stream velocity is represented by $u_e(x) = be^{x/l}$, where $b > 0$. Furthermore, the wall mass transmission is shown by $v_w(x) = v_0 e^{x/2l}$, in which mass suction and injection are indicated by $v_0 > 0$ and $v_0 < 0$, respectively. A strongly applied magnetic field in an exponential form is given by $B(x) = B_0 e^{x/2l}$, which acts perpendicularly to the surface. Considering all these assumptions, we extend the work of [15,23,24], and the proposed mathematical model is given by:

$$\frac{\partial u}{\partial x} + \frac{\partial v}{\partial y} = 0, \tag{1}$$

$$u\frac{\partial u}{\partial x} + v\frac{\partial u}{\partial y} = u_e\frac{du_e}{dx} + \frac{\mu_{nf}}{\rho_{nf}}\left(\frac{\partial^2 u}{\partial y^2}\right) - \frac{\sigma_{nf}}{\rho_{nf}}B_0^2(x)(u - u_e), \tag{2}$$

$$\left(\rho C_p\right)_{nf}\left(u\frac{\partial T}{\partial x} + v\frac{\partial T}{\partial y}\right) = \kappa_{nf}\left(\frac{\partial^2 T}{\partial y^2}\right) + \mu_{nf}\left(\frac{\partial u}{\partial y}\right)^2, \tag{3}$$

with boundary conditions [23,24]:

- at $y = 0$:

$$v = v_w, \quad u = u_w, \quad T = T_w = T_\infty + T_0 e^{2x/l}, \tag{4a}$$

- as $y \to \infty$:

$$u = u_e(x), \qquad T = T_\infty, \tag{4b}$$

where the velocity components along the axial and normal directions are u and v, respectively. Additionally, blood density, viscosity, electrical conductivity and thermal conductivity are denoted by ρ, μ, σ, κ, respectively. The subscript symbol $(\ldots)_{nf}$ indicates a nanofluid, which refers to a base fluid with nanoparticles. The proposed model is shown in Fig. 2.

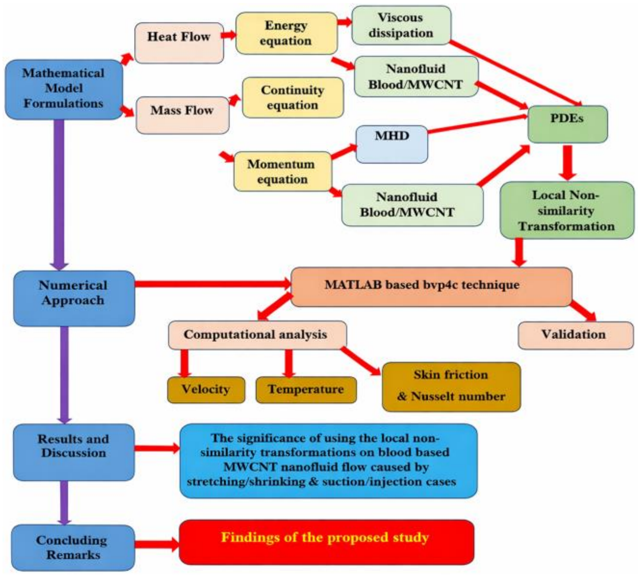

Fig. 1. Flow chart of model simulation.

The effective thermo-physical characteristics of the applied nanofluid model equations are given in [25–28], where ϕ is the particle volume fraction. Additionally, the symbols R_p, h denote the particle radius and interspacing, respectively.

$$\frac{\mu_{nf}}{\mu_{blood}} = 1 + 2.5\phi + 4.5\left[\frac{1}{\frac{h}{R_p}\left(2+\frac{h}{R_p}\right)\left(1+\frac{h}{R_p}\right)^2}\right],$$

$$\rho_{nf} = (1-\phi)\rho_{blood} + \phi\rho_{MWCNT},$$

$$(\rho C_p)_{nf} = (1-\phi)\,(\rho C_p)_{blood} + \phi\,(\rho C_p)_{MWCNT}, \tag{5}$$

$$\frac{\sigma_{nf}}{\sigma_{blood}} = (1-\phi)\sigma_{blood} + \phi\sigma_{MWCNT},$$

$$\frac{\kappa_{nf}}{\kappa_{blood}} = \frac{(\kappa_{MWCNT}+2\,\kappa_{blood}) - 2\phi\,(\kappa_{blood}-\kappa_{MWCNT})}{(\kappa_{MWCNT}+2\,\kappa_{blood}) + \phi\,(\kappa_{blood}-\kappa_{MWCNT})}.$$

To mathematically handle this proposed model, the following nonsimilarity flow is introduced [29,30]:

$$\xi = e^{x/l}, \qquad \eta = \sqrt{\frac{b}{2\upsilon_f l}}\, y e^{x/2l},$$

$$\theta(\xi,\eta) = \frac{T-T_\infty}{T_w-T_\infty}, \qquad u = be^{x/l} f'(\xi,\eta), \tag{6}$$

$$v = -\sqrt{\frac{b\upsilon_f}{2l}}\, e^{x/2l}\left(\eta f'(\xi,\eta) + f(\xi,\eta) + 2\xi\frac{\partial f}{\partial \xi}\right),$$

where ξ is known as a nonsimilarity variable, while η is known as a pseudosimilarity variable.

Equations (2) and (3) are reduced into the following nonsimilar system through the use of Eqs. (5) and (6) as follows:

$$A_1 f''' + f f'' - 2\left(f'^2 - 1\right) - 2A_2 M(f'-1) +$$
$$-2\xi\left[f'\frac{\partial^2 f}{\partial\xi\partial\eta} - f''\frac{\partial f}{\partial \xi}\right] = 0 \tag{7}$$

$$A_3 A_4\,\theta'' + Pr\left[A_4 A_5 \mathrm{Ec} f''^2 + f\theta' - 4\theta f'\right] +$$
$$-2\,\mathrm{Pr}\,\xi\left[f'\frac{\partial\theta}{\partial\xi} - \theta'\frac{\partial f}{\partial\xi}\right] = 0, \tag{8}$$

along with:

$$f(\xi,0) + 2\xi\frac{\partial f}{\partial\xi} = S, \quad f'(\xi,0) = \lambda, \quad \theta(\xi,0) = 1,$$
$$f'(\xi,\infty) \to 0, \qquad \theta(\xi,\infty) \to 0, \tag{9}$$

where prime $(\ldots)'$ denotes the derivatives concerning η.

Additionally, the physical nondimensional parameters are given in Table 1.

Table 1. Physical parameters.

Parameter	Expression
Stretching/shrinking parameter	$\lambda = \frac{b}{c}$ Stretching whenever: $\lambda > 0$ Shrinking whenever: $\lambda < 0$ Static whenever: $\lambda = 0$
Suction/injection parameter	$S = -\sqrt{\frac{2l}{b\upsilon_f}}\, v_0$ Suction whenever: $S > 0$ Injection whenever: $S < 0$
Magnetic field parameter	$M = \frac{B_0^2\sigma_f l}{b\rho_f}$
Prandtl number	$\mathrm{Pr} = \frac{\upsilon_f}{\alpha_f}$
Eckert number	$\mathrm{Ec} = \frac{b^2}{T_0 (\rho C_p)_f}$
Local Reynolds number	$\mathrm{Re} = \frac{bl}{\upsilon_f}$

Additionally, we have:

$$A_1 = \frac{1+2.5\phi+4.5\left[\frac{1}{\frac{h}{R_p}\left(2+\frac{h}{R_p}\right)\left(1+\frac{h}{R_p}\right)^2}\right]}{\left(1-\phi+\phi\frac{\rho_{MWCNT}}{\rho_{blood}}\right)}, \qquad A_2 = \frac{\left(1-\phi+\phi\frac{\sigma_{MWCNT}}{\sigma_{blood}}\right)}{\left(1-\phi+\phi\frac{\rho_{MWCNT}}{\rho_{blood}}\right)},$$

$$A_3 = \frac{\kappa_{nf}}{\kappa_{blood}}, \qquad A_4 = \frac{1}{\left(1-\phi+\phi\frac{(\rho C_p)_{MWCNT}}{(\rho C_p)_{blood}}\right)},$$

$$A_5 = 1 + 2.5\phi + 4.5\left[\frac{1}{\frac{h}{R_p}\left(2+\frac{h}{R_p}\right)\left(1+\frac{h}{R_p}\right)^2}\right].$$

Two important physical quantities under the proposed model are the skin friction parameter and the local Nusselt number:

$$(2\mathrm{Re})^{-\frac{1}{2}} C_f = \frac{A_1}{\xi} f'' f(\xi,0),$$

$$(2\mathrm{Re})^{-\frac{1}{2}} \mathrm{Nu} = -\xi\theta'(\xi,0). \tag{10}$$

3. Numerical procedure and validation

3.1. Local similarity technique

It was suggested that the nonsimilar boundary layers may be solved by applying a local nonsimilarity approach, which was initially presented by Minkowycz and Sparrow [28] and then developed by [29–32]. The local similarity form of Eqs. (7) and (8) associated with boundary conditions is obtained as follows by removing the terms associated with $\partial f/\partial\xi$ and $\partial\theta/\partial\xi$:

$$A_1\, f''' + f\, f'' - 2\left(f'^2 - 1\right) - 2A_2 M(f' - 1) \;= 0, \quad (11)$$

$$A_3 A_4\ \theta'' + \mathrm{Pr}\left[A_4 A_5 \mathrm{Ec} f''^2 + f\theta' - 4\theta\ f'\right] = 0, \quad (12)$$

along with:

$$(\xi,0) + 2\xi\frac{\partial f}{\partial\xi} = S, \qquad f'(\xi,0) = \lambda, \qquad \theta(\xi,0) = 1,$$
$$f'(\xi,\infty)\ \to 0, \qquad \theta(\xi,\infty) \to 0 \quad (12)$$

3.2. Local nonsimilarity technique

3.2.1. First truncation level

To achieve first-level truncation, Eqs. (7)–(8) are kept without approximation and substituted:

$$\begin{cases} g = \dfrac{\partial f}{\partial\xi} \\ m = \dfrac{\partial\theta}{\partial\xi}\cdot \end{cases} \quad (14)$$

Therefore, one can obtain:

$$A_1\, f''' + f\, f'' - 2\left(f'^2 - 1\right) - 2A_2 M(f' - 1) +$$
$$-2\xi[\ f'g' - gf''] \;= 0 \quad (15)$$

$$A_3 A_4\ \theta'' + Pr\left[A_4 A_5 \mathrm{Ec} f''^2 + f\theta' - 4\theta\ f'\right] +$$
$$-2\,\mathrm{Pr}\,\xi\ \ [f'm - \theta' g] = 0, \quad (16)$$

along with:

$$f(\xi,0) + 2\xi g = S, \qquad f'(\xi,0) = \lambda, \qquad \theta(\xi,0) = 1$$
$$f'(\xi,\infty)\ \to 0, \qquad \theta(\xi,\infty) \to 0 \quad (17)$$

3.2.2. Second truncation level

Now, we differentiate with respect to ξ and remove all the terms $\frac{\partial g(\eta,\xi)}{\partial\xi}$, $\frac{\partial m(\eta,\xi)}{\partial\xi}$ and their derivatives. In light of the above, the system of the 2nd truncation level contains Eq. (18)–(20):

$$A_1\ g''' + f\ g'' + 3g\ f'' - 6f'g' - 2A_2 M g' +$$
$$-2\xi\left[\ g'^2 - gg''\right] \;= 0, \quad (18)$$

$$\mathrm{Pr}[2A_4 A_5 \mathrm{Ec} f'' g'' + f\ m' - 6mf' + 3\theta' g - 4\theta\ g'] +$$
$$-2\,\mathrm{Pr}\,\xi\ \ [g'm - m'g] + A_3 A_4\ m'' = 0 \quad (19)$$

with the following BCs:

$$g(\xi,0) = 0, \qquad g'(\xi,0) = 0, \qquad m(\xi,0) = 0$$
$$g'(\xi,\infty)\ \to 0, \qquad m(\xi,\infty) \to 0. \quad (20)$$

4. Results and discussion

This section presents a visual representation of the computational results of the physical parameters that affect the fluid velocity, temperature, skin friction and Nusselt number. We used the bvp4c approach, which is based on MATLAB, to handle this computationally. Table 2 also presents a comparison with existing research to determine the accuracy of the numerical approach used, which was determined to be within acceptable bounds. Additionally, this study used MWCNT particles to simulate blood numerically. Consequently, we conducted further research [34–37] and considered the information shown in Table 3 to produce realistic simulations.

Table 2. Comparison of values of $f''(0)$ when $M = \varphi = \xi = \mathrm{Ec} = 0$, $\lambda = 1$, Pr = 7 for various values of S.

S	Present outcomes (local nonsimilarity solutions)	Gorla and Sidawi [33]
–0.7	–0.72250	–0.72252
–0.4	–0.83418	–0.83420
0.0	–1.01441	–1.01435
0.4	–.2313	–1.23180
0.7	–1.41879	–1.41884

Table 3. Physical properties of blood and MWCNTs.

Properties	Base fluid: blood	Nanoparticles MWCNT
C_p (J kg^{-1} K^{-1})	3.9×10^3	796
ρ (kg m^{-3})	1050	1600
σ (s m^{-1})	0.8	1.9×10^{-4}
κ (W m^{-1} K^{-1})	0.5	3.7

In this study, we present a comprehensive comparison of the following:

(i) blood/MWCNT behaviour in the stretched case,
(ii) blood/MWCNT behaviour in the shrinking case.

Figures 3 and 4 illustrate the influence of the magnetic field parameter on the velocity and temperature profiles for both the stretching and shrinking cases. Increasing the magnetic field parameter reduces the fluid velocity while increasing the temperature distribution. This behaviour is attributed to the Lorentz force generated by the interaction between the magnetic field and the electrically conducting nanofluid, which acts as a resistive force opposing the fluid motion and suppressing the velocity field. The reduced fluid motion weakens convective heat transport and promotes thermal energy accumulation within the boundary layer, resulting in an increase in the temperature profile.

Figures 5 and 6 illustrate the effects of nanoparticle volume fraction on the velocity and temperature profiles. Increasing the volume fraction reduces the fluid velocity while enhancing the

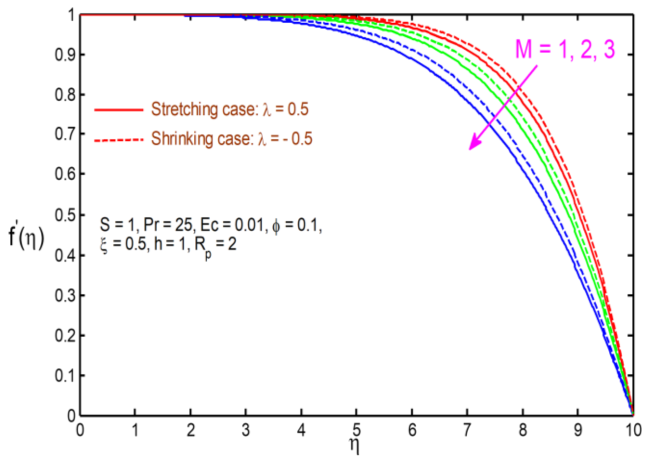

Fig. 3. Influence of M on $f'(\eta)$.

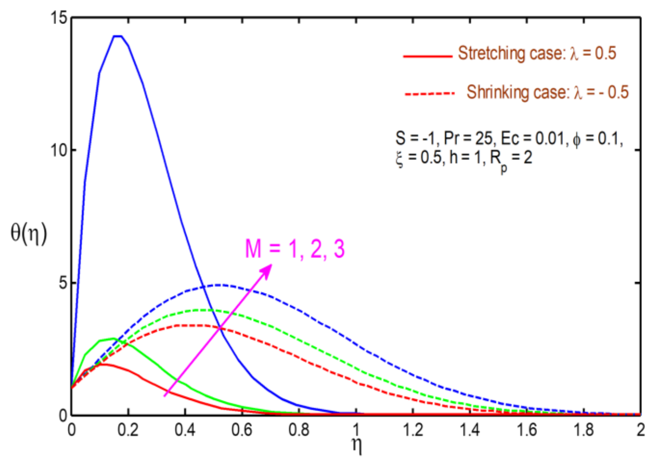

Fig. 4. Influence of M on $\theta(\eta)$.

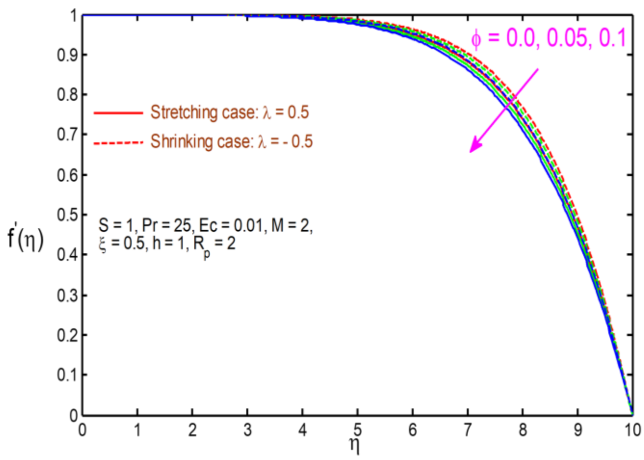

Fig. 5. Influence of ϕ on $f'(\eta)$.

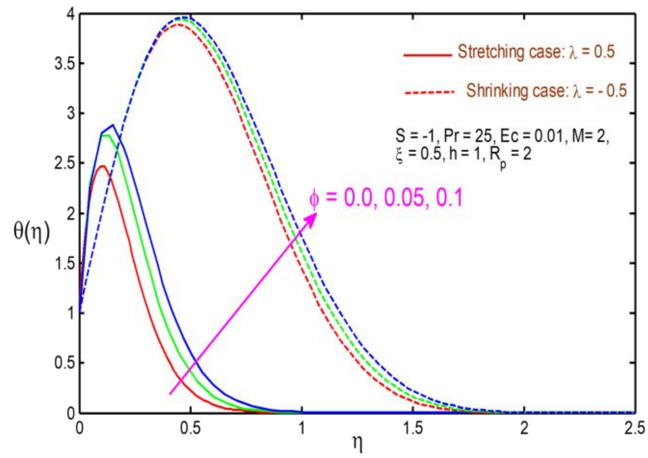

Fig. 6. Influence of ϕ on $\theta(\eta)$.

temperature distribution. The reduction in velocity occurs because the addition of nanoparticles increases the effective viscosity of the nanofluid, which strengthens the momentum resistance within the boundary layer. Conversely, the temperature increases since a higher nanoparticle concentration improves the effective thermal conductivity of the nanofluid, thereby increasing heat transport within the fluid.

Figures 7 and 8 present the influence of the particle spacing on the velocity and temperature distributions. Increasing the particle spacing enhances both the velocity and temperature profiles. Physically, a larger interparticle spacing reduces nanoparticle–nanoparticle interactions and agglomeration effects, which promotes more uniform dispersion of nanoparticles within the base fluid. This improved dispersion facilitates more efficient mo-

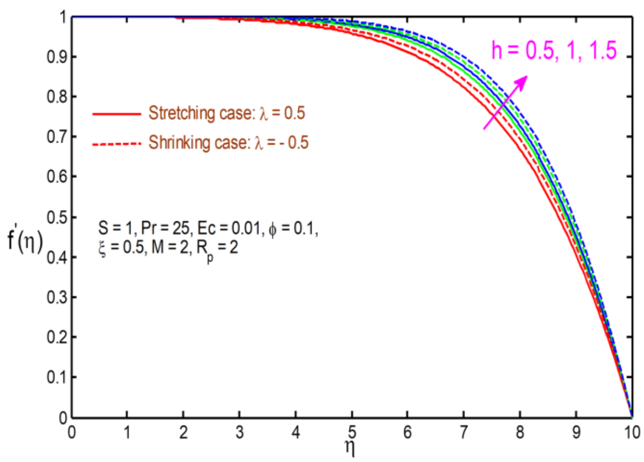

Fig. 7. Influence of h on $f'(\eta)$.

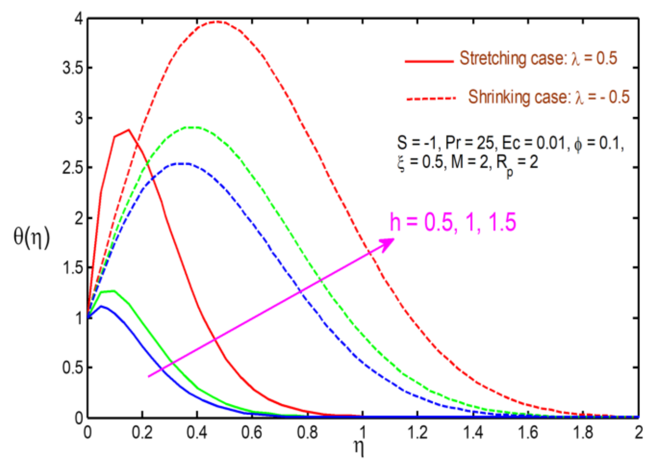

Fig. 8. Influence of h on $\theta(\eta)$.

mentum and heat transport within the boundary layer, resulting in enhanced velocity and temperature distributions.

Figures 9 and 10 illustrate the influence of the particle radius on the velocity and temperature distributions. Increasing the particle radius decreases the velocity profile while enhancing the temperature distribution. The reduction in velocity is attributed to the increase in effective viscosity and particle inertia associated with larger nanoparticles, which strengthens the momentum resistance within the boundary layer. Conversely, the temperature increases because larger particles increase the effective thermal conductivity of the nanofluid, promoting improved heat transport within the fluid.

Finally, Figs. 11 to 16 examine variations of the skin friction and local Nusselt number with physical parameters such as the particle radius, particle volume fraction and magnetic field.

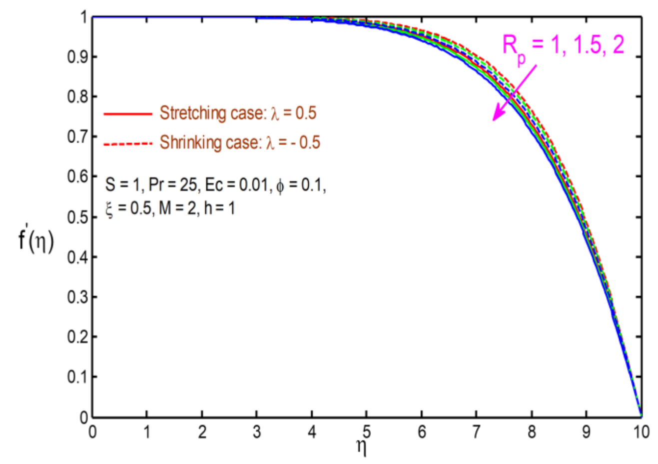

Fig. 9. Influence of R_p on $f'(\eta)$.

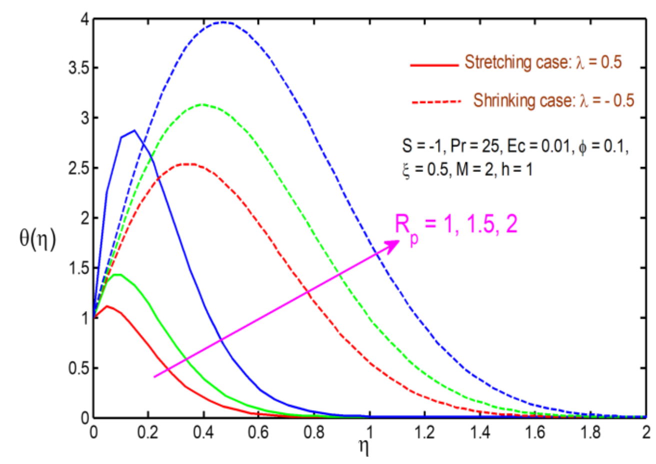

Fig. 10. Influence of R_p on $\theta(\eta)$.

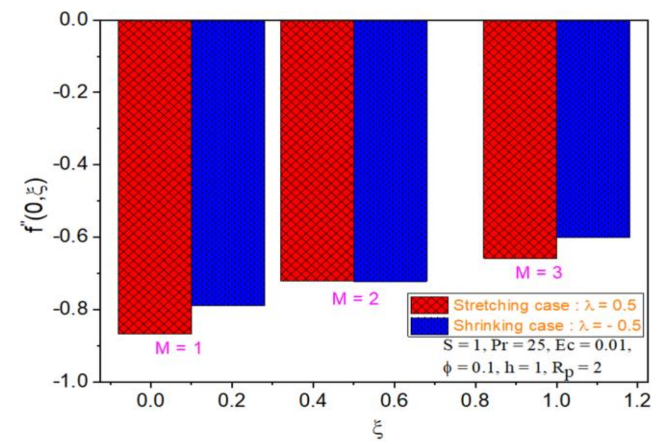

Fig. 11. Influence of M on $f''(0, \xi)$ against ξ.

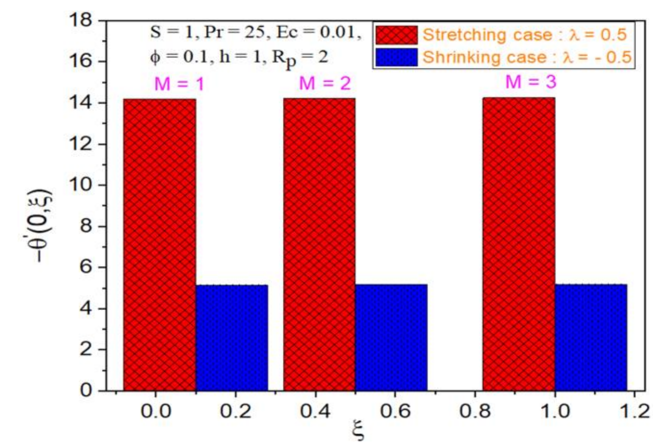

Fig. 12. Influence of M on $-\theta'(0, \xi)$ against ξ.

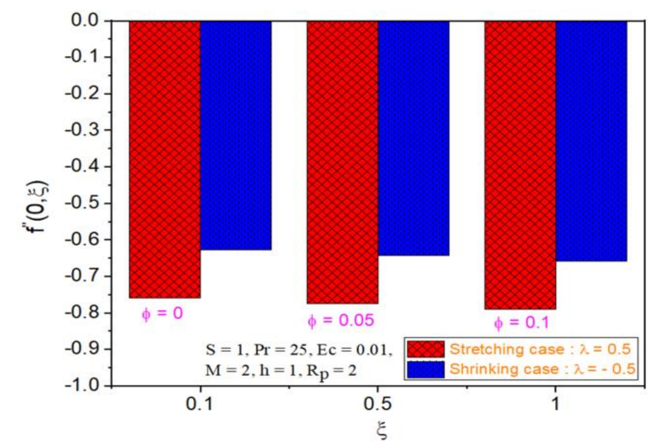

Fig. 13. Influence of ϕ on $f''(0, \xi)$ against ξ.

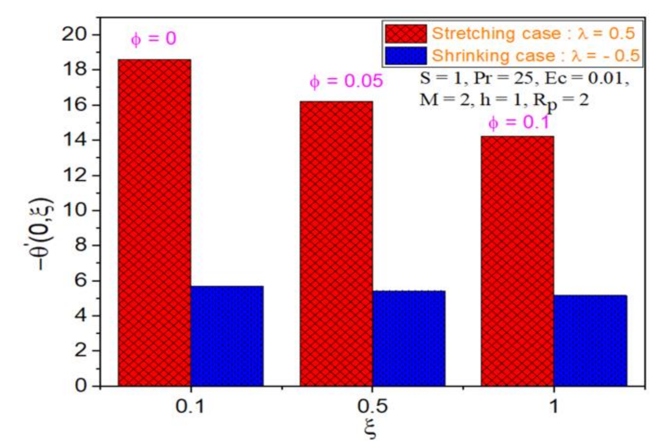

Fig. 14. Influence of ϕ on $-\theta'(0, \xi)$ against ξ.

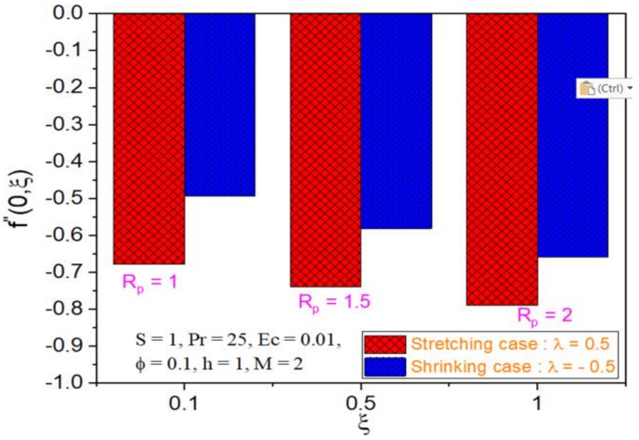

Fig. 15. Influence of R_p on $f''(0, \xi)$ against ξ.

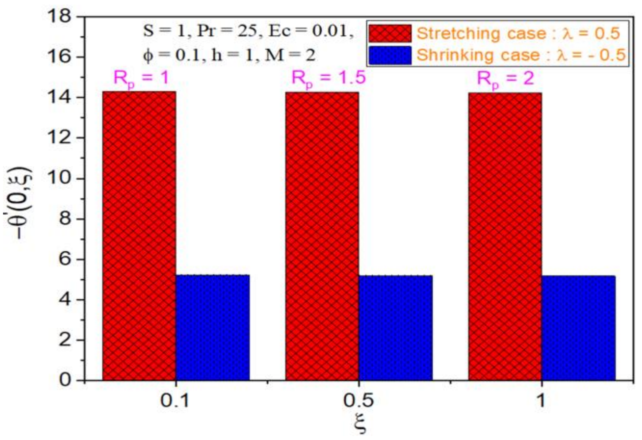

Fig. 16. Influence of R_p on $-\theta'(0, \xi)$ against ξ.

According to the study, for both the stretching and shrinking scenarios, the magnetic field parameter improves both the skin friction and the Nusselt number. The skin friction is shown to improve by 24.15% in the stretching case and by 23.9% in the shrinking case over a range of magnetic field parameter values from 1 to 3, whereas the Nusselt number improves by 0.36% and 0.68% for the stretching and shrinking situations, respectively. Both the skin friction and the Nusselt number decrease as the particle radius increases. The skin friction decreases by 16.52% and 33.18% for the stretching and shrinking scenarios, respectively, for particle radius values ranging from 1 to 2. The Nusselt number values are decreased by 0.53% and 0.96%, respectively, for the stretching and shrinking scenarios. The skin friction and Nusselt number decrease as the particle volume fraction increases from 0 to 0.1. According to the study, the skin friction decreases by approximately 4.2% in the stretching case and by approximately 4.97% in the shrinking case. The Nusselt number likewise shows a noticeable shift, decreasing by approximately 23.46% and 8.83%, respectively, in the stretching and shrinking scenarios.

5. Conclusions

The present study investigated the nonsimilar flow and heat transfer characteristics of a biomagnetic blood-based MWCNT nanofluid over an exponentially stretched/shrinking sheet under the influence of magnetic field, particle radius, particle volume fraction and particle spacing. The governing equations were solved via the local nonsimilarity technique with the MATLAB bvp4c solver. The key findings are summarised as follows:

- The velocity profile decreases significantly with increasing magnetic field parameters, particle radius and particle volume fraction, whereas the temperature profile increases under the same conditions for both the stretching and shrinking cases.
- Increasing the particle spacing enhances both the velocity and temperature distributions, indicating improved nanoparticle dispersion within the base fluid.
- The skin friction coefficient increases by approximately 24.15% in the stretching case and 23.9% in the shrinking case when the magnetic field parameter increases within the considered range.
- The heat transfer rate (Nusselt number**)** decreases by approximately 23.46% and 8.83% for the stretching and shrinking cases, respectively, when the nanoparticle volume fraction increases from 0 to 0.1.
- Increasing the particle radius from 1 to 2 reduces the skin friction coefficient by approximately 16.52% in the stretching case and 33.18% in the shrinking case, while also slightly decreasing the Nusselt number.

From a practical perspective, the results indicate that magnetic control and nanoparticle characteristics can significantly influence heat transfer behaviour in biomagnetic nanofluid systems**,** which may be useful in biomedical engineering applications such as magnetic drug delivery, targeted thermal therapy and microscale cooling technologies.

Although the present analysis provides useful insight into biomagnetic nanofluid transport, the model is developed under simplified assumptions such as constant thermophysical properties, Newtonian fluid behaviour, and steady laminar flow conditions. In real biomedical environments, additional phenomena such as ferrohydrodynamic (FHD) interactions, variable viscosity and thermal conductivity, non-Newtonian blood rheology, and radiative heat transfer may significantly affect the flow and heat transfer characteristics. The incorporation of these effects in future studies would provide a more realistic description of biomagnetic nanofluid transport in biomedical and microscale thermal systems.

References

[1] Saeed, A., Alsubie, A., Kumam, P., Nasir, S., Gul, T., & Kumam, W. (2021). Blood based hybrid nanofluid flow together with electromagnetic field and couple stresses. *Scientific Reports*, 11, 12865. doi: 10.1038/s41598-021-92186-z

[2] Alanazi, M.M., Hendi, A.A., Raza, Q., Rehman, M.A., Qureshi, M.Z.A., Ali, B., & Shah, N.A. (2023). Numerical computation of hybrid morphologies of nanoparticles on the dynamic of nanofluid: The case of blood-based fluid. *Axioms*, 12, 163. doi: 10.3390/axioms12020163

[3] Mohamed, M.K.A., Yasin, S.H.M., Salleh, M.Z., & Al-kasasasbeh, H.T. (2021). MHD stagnation point flow and heat transfer over a stretching sheet in a blood-based Casson ferrofluid with Newtonian heating. *Journal of Advanced Research in Fluid*

Mechanics and Thermal Sciences, 82, 1–11 doi: 10.37934/arfmts.82.1.111

[4] Samat, N.A.A., Bachok, N., & Arifin, N.M. (2024). Boundary layer stagnation point flow and heat transfer over a nonlinear stretching/shrinking sheet in hybrid carbon nanotubes under magnetohydrodynamics. *Computation*, 12, 46. doi: 10.3390/computation12030046

[5] Khan, W.A., Khan, Z.H., & Rahi, M. (2014). Fluid flow and heat transfer of carbon nanotubes along a flat plate with Navier slip boundary. *Applied Nanoscience*, 4, 633–641. doi: 10.1007/s13204-013-0242-9

[6] Khan, M.R., Pan, K., Khan, A.U., & Ullah, N. (2020). Comparative study on heat transfer in CNTs–water nanofluid over a curved surface. *International Communications in Heat and Mass Transfer*, 116, 104707. doi: 10.1016/j.icheatmasstransfer.2020.104707

[7] Das, K., Sutradhar, B., & Kundu, P.K. (2024). Impact of nonlinear radiation on an unsteady magneto hybrid nanofluid flow over an upward/downward rotating disk. *Numerical Heat Transfer, Part A*, 85, 2664–2681. doi: 10.1080/10407782.2023.2228477

[8] Priyadharshini, P., & Archana, M.V. (2025). Artificial neural networks computing system for Ree–Eyring hybrid nanofluid flow over a solar panel sheet: Hamilton–Crosser model. *International Journal of Ambient Energy*, 46, 2451212. doi: 10.1080/01430750.2025.2451212

[9] Rehman, A., Khan, I.A., Abualnaja, K.M., Ali, H.E., Jan, R., & Mahmoud, E.E. (2025). Analytical simulation of Darcy–Forchheimer MHD flow of CNT nanofluids over a stretching/shrinking surface with variable viscosity and slip conditions. *Journal of the Brazilian Society of Mechanical Sciences and Engineering*, 47, 184. doi: 10.1007/s40430-025-05428-w

[10] Ramanuja, M., Kavitha, J., Sudhakar, A., & Radhika, N. (2023). Study of MHD SWCNT–blood nanofluid flow with viscous dissipation and radiation effects through porous medium. *Journal of the Nigerian Society of Physical Sciences*, 5, 1054–1054. doi: 10.46481/jnsps.2023.1054

[11] Nagaraja, B., Vidhya, K.G., Almeida, F., & Kumar, P. (2025). Numerical illustration of diffusive flow of blood-based tri-hybrid nanofluid generated by a curved stretching sheet using law of porosity. *Numerical Heat Transfer, Part A: Applications*, 86(16), 5626–5647. doi: 10.1080/10407782.2024.2333042

[12] Rehman, A., Khan, D., Jan, R., Aloqaily, A., & Mlaiki, N. (2023). Marangoni convection in stagnation point flow of blood-based CNT nanofluid over an unsteady stretching surface. *International Journal of Thermofluids*, 20, 100470. doi: 10.1016/j.ijft.2023.100470

[13] Nasir, M., Bég, O.A., Al-Dossari, M., Sarhan, N.M., Kuharat, S., Waqas, M., & Daminova, G. (2024). SWCNT/MWCNT-doped thermomagnetic nanoblood boundary layer flow with non-Darcy, chemical reaction, viscous heating and Joule dissipation. *Diamond and Related Materials*, 148, 111447. doi: 10.1016/j.diamond.2024.111447

[14] El Glılı, I., & Drıouıch, M. (2024). Impact of inclined magnetic field on nonorthogonal stagnation point flow of CNT–water through stretching surface in a porous medium. *Journal of Thermal Engineering*, 10(1), 115–129. doi: 10.18186/thermal.1429409

[15] Mahanta, C., & Sharma, R.P. (2024). Collective impact of convective boundary and slip conditions on Casson ternary nanofluid flow over a stretching sheet. *Journal of Thermal Analysis and Calorimetry*, 149, 8391–8408. doi: 10.1007/s10973-024-13146-z

[16] Ahmad, S., Khan, A.A., Khan, M.N., Knani, S., Ahammad, N.A., & Eleesy, I.E. (2025). Energy Transport in Ternary Hybrid Nanofluid with Variable Thermal Conductivity under the Combined Influence of Electroviscous Effect, Electric Potential, and Heat Generation. *Dynamics of Atmospheres and Oceans*, 112, 101619. doi: 10.1016/j.dynatmoce.2025.101619

[17] Yasir, M., Khan, M.N., Ahammad, N.A., Alshaban, E., Hassaballa, A.A., & Elseesy, I.E. (2025). Rheology of thermally nonlinear radiated flow of cross-material induced by shrinking surface: Heat radiation applications. *Journal of Radiation Research and Applied Sciences*, 18(4), 101956. doi: 10.1016/j.jrras.2025.101956

[18] Ahsan, N., Khan, M.N., Aslam, M.N., Saidani, T., Alnfiai, M.M., & Gamaoun, F. (2025). Bio-convective flow of non-Newtonian nanofluid with triple stratification effect over a curved stretching surface. *ZAMM-Journal of Applied Mathematics and Mechanics/Zeitschrift für Angewandte Mathematik und Mechanik*, 105(11), e70280. doi: 10.1002/zamm.70280

[19] Yasir, M., Choubani, K., Khan, M.N., Almeshaal, M.A., & Hussien, M. (2025). Influence of Cattaneo-Christov radiative heat flux in magnetized flow performance of three different materials with variable constraints. *Dynamics of Atmospheres and Oceans*, 112, 101608. doi: 10.1016/j.dynatmoce.2025.101608

[20] Kallem, S.R., Sheri, S.R., Prathiba, A., & Shankar, G. (2025). Numerical analysis of the effect of chemical reaction and heat source on MHD hyperbolic tangent fluid flow across a non-linear stretching sheet in a porous medium. *Archives of Thermodynamics*, 46(2), 57–67. doi: 10.24425/ather.2025.154906

[21] Biswas, N., Mandal, D.K., Manna, N.K., & Benim, A.C. (2025). Thermomagnetic convection and entropy generation in a hybrid nanofluid filled wavy-walled cavity heated non-uniformly. *Archives of Thermodynamics*, 46(1), 61−81. doi: 10.24425/ather.2025.154182

[22] M, A., & De, P. (2025). Electro-osmotic and magnetohydrodynamic flow of Maxwell nanofluid over Darcy-Forchheimer porous medium with Soret-Dufour effects. *Archives of Thermodynamics*, 46(2), 69−81. doi: 10.24425/ather.2025.154907

[23] Magyari, E., & Keller, B. (1999). Heat and mass transfer in boundary layers on an exponentially stretching continuous surface. *Journal of Physics D: Applied Physics*, 32(5), 577. doi: 10.1088/0022-3727/32/5/012

[24] Prakash, O., Rao, P.S., Sharma, R.P., & Mishra, S.R. (2023). Hybrid nanofluid MHD motion towards an exponentially stretching/shrinking sheet with the effect of thermal radiation, heat source and viscous dissipation. *Pramana*, 97(2), 64. doi: 10.1007/s12043-023-02533-0

[25] Ferdows, M., Alam, J., Murtaza, M.G., & Tzirtzilakis, E.E. (2023). Effects of magnetic particle diameter and spacing on biomagnetic flow and heat transfer over a stretched cylinder in presence of magnetic dipole. *Journal of Mechanics in Medicine and Biology*, 23, 2350036. doi: 10.1142/S0219519423500367

[26] Alam, J., & Murtaza, M.G. (2024). Significance of biomagnetic fluid flow with Ni-$ZnFe_2O_4$ particle over a wedge in the presence of a magnetic dipole. *Multiscale and Multidisciplinary Modeling, Experiments and Design*, 7, 5673–5684. doi: 10.1007/s41939-024-00526-z

[27] Alam, J., Murtaza, M.G., Petropoulou, E.N., Tzirtzilakis, E.E., & Ferdows, M. (2023). A parametric simulation of MHD flow and heat transfer of blood–Fe_3O_4 nanofluid over an exponentially stretching cylinder. *BioNanoScience*, 13, 891–899. doi: 10.1007/s12668-023-01141-x

[28] Minkowycz, W.J., & Sparrow, E.M. (1974). Local nonsimilar solutions for natural convection on a vertical cylinder. *Journal of Heat Transfer*, 96(2), 178–183. doi: 10.1115/1.3450161

[29] Mansoor, M., Nawaz, Y., & Ul-Hassan, Q.M. (2022). Nonsimilar method for heat and mass transfer of MHD radiative flow over an

exponentially stretching sheet. *Thermal Science*, 26(5A), 3703–3714. doi: 10.2298/TSCI210505309M

[30] Cui, J., Razzaq, R., Farooq, U., Khan, W.A., Farooq, F.B., & Muhammad, T. (2022). Forced convection analysis of nanofluid flow over a stretching sheet with chemical reaction and heat generation using nonsimilar modeling. *Alexandria Engineering Journal*, 61, 4253–4261. doi: 10.1016/j.aej.2021.09.045

[31] Ferdows, M., Barmon, A., Bég, O.A., Shamshuddin, M.D., & Sun, S. (2023). Nonisothermal electroconductive radiative stretching boundary layer heat transfer with aligned magnetic field: A local nonsimilar solution. *Applied Sciences*, 13(7), 4592. doi: 10.3390/app13074592

[32] Razzaq, R., & Farooq, U. (2021). Nonsimilar forced convection analysis of Oldroyd-B fluid flow over an exponentially stretching surface. *Advances in Mechanical Engineering*, 13(7). doi: 10.1177/16878140211034604

[33] Gorla, R.S.R., & Sidawi, I. (1994). Free convection on a vertical stretching surface with suction and blowing. *Applied Scientific Research*, 52, 247–257. doi: 10.1007/BF00853952

[34] Tzirtzilakis, E.E. (2005). A mathematical model for blood flow in magnetic field. *Physics of Fluids*, 17, 077103. doi: 10.1063/1.1978807

[35] Tzirtzilakis, E.E., & Tanoudis, G.B. (2003). Numerical study of biomagnetic fluid flow over a stretching sheet with heat transfer. *International Journal of Numerical Methods for Heat and Fluid Flow*, 13(7), 830–848. doi: 10.1108/09615530310502055

[36] Alam, J., Murtaza, M.G., Petropoulou, E.N., Tzirtzilakis, E.E., & Ferdows, M. (2022). Group-theoretical simulation of biomagnetic fluid flow and heat transfer with Fe_3O_4 particles under thermal radiation and magnetic dipole. *Mathematics*, 10(19), 3520. doi: 10.3390/math10193520

[37] Alkasasbeh, H.T., Swalmeh, M.Z., Bani Saeed, H.G., Al Faqih, F.M., & Talafha, A.G. (2020). Investigation on CNTs–water and human blood-based Casson nanofluid flow over a stretching sheet under impact of magnetic field. *Frontiers in Heat and Mass Transfer*, 14, 1–7. doi:10.5098/hmt.14.15